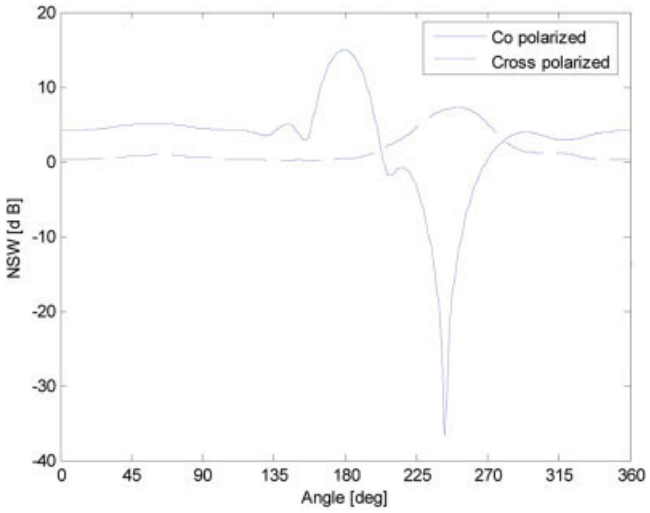

Figure 4 Scattering width of the circular cylinder $Z_{zz}(\phi) = 200\sin(\phi) + i150\cos(3\phi)$, $Z_{z\phi}(\phi) = -5\phi^2\sin(2\phi) - i200e^{-\phi}$, $Z_{\phi\phi}(\phi) = -5\phi^2 - i30\phi$, $Z_{\phi} = 40\phi + i30\phi\sin(3\phi)$, $\phi_0 = 0$, $a = \lambda$, $N = 30$. [Color figure can be viewed in the online issue, which is available at www.interscience.wiley.com]

in Figure 4. In all cases, frequency is selected as 33 MHz, angle of incidence $\phi_0 = 0$ and exterior medium is assumed to be free space.

4. CONCLUSIONS

In this study, scattering from inhomogeneous anisotropic impedance cylinder for TM incidence is investigated analytically. Similar procedure can also be applied for TE incidence case. Investigated boundary condition is the most general condition that contains all boundary condition which have been previously investigated in literature. Both proposed method and Nyström technique are applied for scattering from isotropic inhomogeneous impedance cylinder. Obtained results are compared by those obtained by numeric Nyström technique [10], as seen from Figures 2 and 3, good agreements are observed. Two possible practical application are that proposed method can be used for obtaining desired SW pattern of cylindrical structures or obtaining desired gain and polarization pattern of reflector antennas by choosing appropriate anisotropic surface impedance function.

REFERENCES

1. M.A. Leontovich, Investigations of radio wave propagation-Part 2, Academy of Sciences, USSR, 1948.
2. J.R. Wait, The scope of impedance boundary conditions in radio propagation, IEEE Trans Geosci Remote Sens GRS-28 (1990), 721–723.
3. T.B.A. Senior and J.L. Volakis, Approximate boundary conditions in electromagnetics, The Institutions of Electrical Engineers, London, 1995.
4. D.J. Hoppe and Y. Rahmat-Samii, Impedance boundary conditions in electromagnetics, Taylor and Francis, 1995.
5. T.B.A. Senior, J.L. Volakis, and S.R. Legualt, Higher order impedance and absorbing boundary conditions, IEEE Trans Antennas Propagat 45 (1997), 107–114.
6. N.S. Tezel and S. Paker, Electromagnetic scattering from cylinder described by high-order inhomogeneous impedance boundary conditions, Microwave Opt Technol Lett 48 (2006), 1148–1151.
7. A. Yapar, H. Sahinturk, and I. Akduman, Electromagnetic scattering by an inhomogeneous impedance cylinder, AEU 56 (2002), 3.
8. E. Topsakal, A. Buyukaksoy, and M. Idemen, Scattering of electromagnetic waves by a rectangular impedance cylinder, Wave Motion 31 (2000), 273–296.
9. J.M.L. Bernard and M.A. Lyalinov, Electromagnetic scattering by a smooth convex impedance cone, IMA J Appl Math 69 (2004), 285–333.
10. I. Akduman and R. Kress, Direct and inverse scattering problems for inhomogeneous impedance cylinders of arbitrary shape, Radio Sci (2003).
11. J.A. Kong, Electromagnetic wave theory, 2nd ed., Wiley, New York, NY, 1990.

A REAL-TIME MONITORING PHOTOPOLARIMETER BASED ON A MULTICHANNEL SIGNAL PROCESS SYSTEM

Ruey-Ching Twu
Department of Electro-Optical Engineering, Southern Taiwan University of Technology, Tainan 710, Taiwan, Republic of China; Corresponding author: rctwu@mail.stut.edu.tw

Received 23 May 2007

ABSTRACT: *This study developed and evaluated a photopolarimeter based on a polarization interferometer with four photo detectors. By using the proposed multichannel signal process system, the time varying polarization states of an incident light beam, modulated by an electrically driving liquid crystal cell, can be measured instantly and monitored continually. Research findings contribute to the study of dynamic behaviors of the liquid crystal cell.* © 2007 Wiley Periodicals, Inc.
Microwave Opt Technol Lett 49: 3093–3096, 2007; Published online in Wiley InterScience (www.interscience.wiley.com). DOI 10.1002/mop.22947

Key words: *real-time monitoring; photopolarimeter; polarization interferometry; liquid crystal cell*

1. INTRODUCTION

In the field of optical metrology, measurements of the polarization states of a light beam provide many crucial applications for precise measurements, liquid crystal displays (LCDs), ellipsometers, and surface plasmon resonance (SPR) sensors [1–4]. A photopolarimeter based on a polarization interferometry is the most available set-up used to measure polarization states of the light wave. To save measurement time and increase testing throughput, there are many techniques to achieve a real-time measurement on different polarization states. Among these techniques, a measurement set-up with multiple photo detectors is most likely to fulfill such requirements [3, 5], because it does not need to use time limited mechanically controlling schemes or complex calculations based on received harmonic signals via the Fourier analysis [6]. Meanwhile, the real-time monitoring photopolarimeter can provide a feed-back signal to control process conditions as being used in a thickness monitor for an etching or a deposition machine [3].

This study conducted an experiment that examines the proposed photopolarimeter consisting of a polarization interferometer and a multichannel signal process system (MCSPS). To evaluate functionalities of real-time measurement and continually monitor the dynamic evolutions of polarization states, the study used a LC cell with electronic driving to control polarization sates of the incident light. Many researches have found that dynamic characteristics of LC molecules affect qualities of viewing angle and

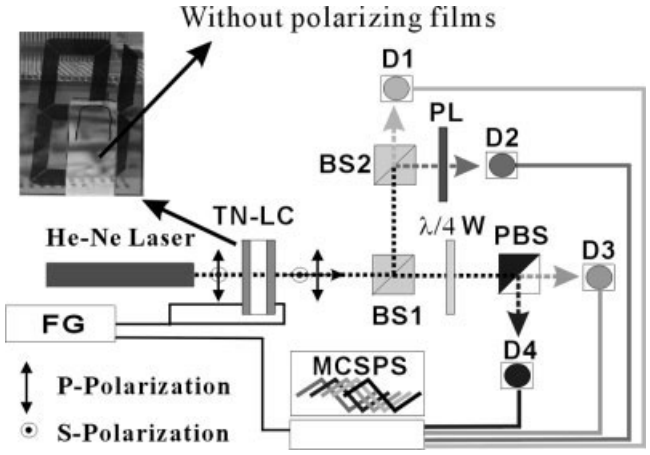

Figure 1 Experimental set-up for a real-time monitoring photopolarimeter

contrast in the LCDs. The corresponding polarization parameters of azimuth angle and phase delay can provide the detailed information about designs of the LC cell including cell gaps and rubbing directions [7]. Moreover, the LC cell is a good phase modulator for wide applications in optical communications and phase shifting interferometers [7, 8]. Consequently, it is important to develop a continually monitoring instrument that determines long-term dynamic behaviors of the LC cell.

2. THEORETICAL ANALYSIS AND EXPERIMENTS

The graphic view of the proposed photopolarimeter is shown in Figure 1. The inset of Figure 1 also presents one segment of a commercial seven-segment TN-LC panel without the covered polarizing films, used to dynamically control the polarization states of the incident light. After passing through the electrically modulated TN-LC cell, the incident light introduces a polarization angle rotation and a phase delay between the horizontally (*p*-polarization) and vertically (*s*-polarization) polarized components of the light. The time-varying polarization sates can then be expressed by the Jones vector

$$E_{\mathrm{lc}} = E_0\begin{pmatrix}\cos\theta(t)\\ \sin\theta(t)\exp^{j\varphi(t)}\end{pmatrix} \tag{1}$$

where, E_0 is the electrical field amplitude of the exiting light from the TN-LC cell, $\theta(t)$ and $\varphi(t)$ are the time-dependent polarization state parameters of azimuth angle and phase delay, respectively. The incident linearly polarized light at 632 nm is from a He-Ne laser. Its polarized axis is oriented as the same direction as the director axis of the TN-LC cell. After passing through the TN-LC cell, the modulated light first enters the nonpolarizing beam splitter (BS1), then separating into the transmitted and reflected directions. The reflected light enters the nonpolarizing beam splitter (BS2), one of the splitting light beams detected directly by a photo detector D1, another one pass through the polarizer (PL) then receiving by a photo detector D2. The transmitted light passes through the λ/4 wave plate (λ/4 W) with axes at 45° with respect to the horizontal laboratory reference frame, and enters the polarizing beam splitter (PBS). Two output polarized lights detected by detectors of *D*3 and *D*4, respectively. This study uses the notations of *P*1, *P*2, *P*3, and *P*4 to represent the amplitudes of electric signal for *D*1, *D*2, *D*3, and *D*4, respectively. Consider in an ideal case (no reflection and perfect elements), the relations between four power signals (*P*1 to *P*4) and the polarization parameters of $\theta(t)$ and $\varphi(t)$ based on the Jones matrix calculations can be expressed as below

$$P1 = \frac{1}{4}E_0^2 \tag{2}$$

$$P2 = \frac{1}{4}E_0^2\cos^2\theta(t) \tag{3}$$

$$P3 = \frac{1}{2}E_0^2\cdot\left[\frac{1}{2} + \sin\theta(t)\cos\theta(t)\sin\varphi(t)\right] \tag{4}$$

$$P4 = \frac{1}{2}E_0^2\cdot\left[\frac{1}{2} - \sin\theta(t)\cos\theta(t)\sin\varphi(t)\right] \tag{5}$$

$$\theta(t) = \cos^{-1}\sqrt{\frac{P2}{P1}} \tag{6}$$

$$\varphi(t) = \sin^{-1}\left[\frac{(P3 - P4/P3 + P4)}{\sin 2(\cos^{-1}\sqrt{P2/P1})}\right] \tag{7}$$

where, the $\theta(t)$ and $\varphi(t)$ can be easily determined according to the formulas (6) and (7), respectively. In experimental arrangements, optical power can be received and converted into electronic signals of voltage via amplified photo detectors (PDA520, THORLABS, USA). Four optical signals and one input voltage signal from a function generator were connected to the MCSPS (see Fig. 2), which consists of a multichannel signal input box (BNC 2120, National Instruments, USA), a shielding signal cable, a data acquisition (DAQ) card (DAQ-6036E, National Instruments, USA), and a laptop computer. LabVIEW software (Version 7.0, National Instruments, USA) provides mathematic and graphic functions to record input signals and measure polarization parameters, displayed continually on a laptop computer.

3. RESULTS AND DISCUSSION

Figure 3 includes three charts that show input signals, measured $\theta(t)$ and $\varphi(t)$, which can be simultaneously found at the display. As shown in Figure 3(a) [similar to Figs. 4(a) and 5(a)], four received signals (as represented by *P*1, *P*2, *P*3, *P*4) and input electrical one (as represented by *V*) as a function of time can be found continually at the same chart, which clearly demonstrates the dynamic

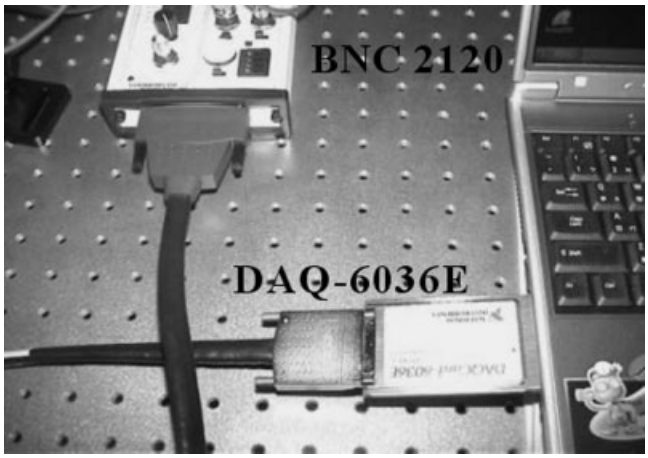

Figure 2 Photograph of the proposed multichannel signal process system

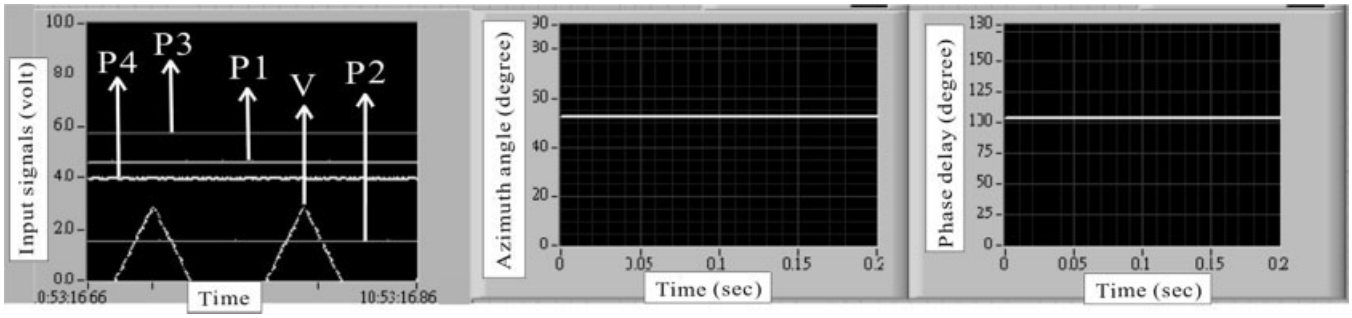

Figure 3 (a) The received signals as a function of time ($V_p = \pm 3$ V, $f = 10$ Hz); (b) The measured azimuth angle versus time; (c) The measured phase delay versus time

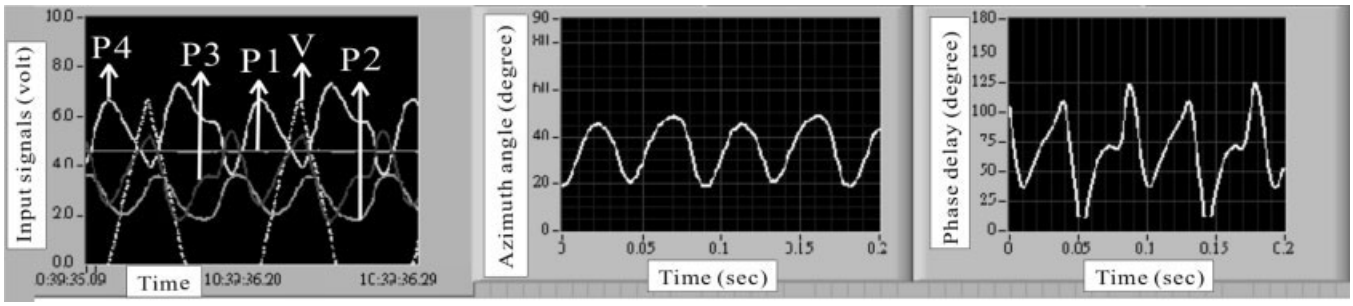

Figure 4 (a) The received signals as a function of time ($V_p = \pm 7$ V, $f = 10$ Hz); (b) The measured azimuth angle versus time; (c) The measured phase delay versus time

relationships between applied voltages and optical power variations on each port. In the measurement conditions of applied triangular voltages with peak value V_p of ± 3 V and modulation frequency f of 10 Hz, respectively. The initial azimuth angle [Fig. 3(b)] and phase delay [Fig. 3(c)] are 46° and 103°, respectively. It means that applied voltages are still below threshold value ($V_p = \pm 4$ V at $f = 10$ Hz) to make LC director starting rotation. Therefore, four optical signals are constant. After the applied voltage exceeds the threshold voltage, LC directors are reoriented by electric fields. Figure 4 further shows dynamic polarization states with various measurement conditions ($V_p = \pm 7$ V, $f = 10$ Hz). A higher voltage forces the LC director alignment to change the direction of electric field, which cause the smaller azimuth angle and phase delay as shown in Figures 4(b) and 4(c), respectively. Figure 5 provides the results using a higher signal frequency ($V_p = \pm 7$ V, $f = 20$ Hz). The variations of the azimuth angle and phase delay are slightly decreased since LC molecules can not completely follow modulated voltages as shown in Figures 5(b) and 5(c). Based on experimental results, measurement response is mainly determined by the sampling rate of the used DAQ card. In case of sampling rate of 300 kHz shared with five input channels, each of five channels has a sampling rate around 60 kHz and can provide time resolutions of about 15 μs, which is enough for measuring the TN-LC cells. The system's measurement response can be improved by choosing a higher sampling rate DAQ card as well as provide important implications for remote data acquisition, analysis, design and distributed control.

4. CONCLUSION

In sum, this study developed and tested a real-time monitoring photopolarimeter consisting of a polarization interferometer and a MCSPS. Research findings successfully demonstrated capacities of continue analysis and in-situ display for polarization states of an incident light modulated by a TN-LC cell under applied voltages. The measurement apparatus designed by this study will be useful

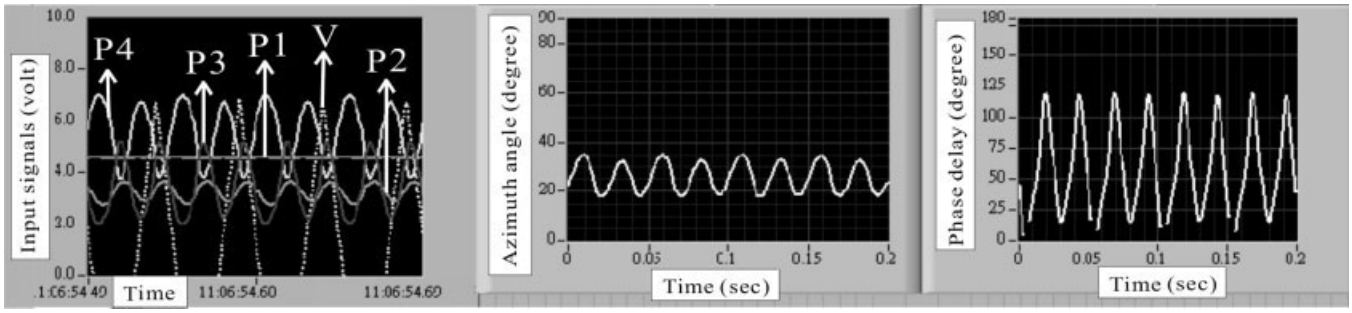

Figure 5 (a) The received signals as a function of time ($V_p = \pm 7$ V, $f = 20$ Hz); (b) The measured azimuth angle versus time; (c) The measured phase delay versus time

to enhance an understanding of dynamical behaviors of LC cells under an external influence.

ACKNOWLEDGMENT

This work was partially supported by the National Science Council, Taiwan, R.O.C., under grant no. NSC 92–2218-E-218–020.

REFERENCES

1. X. Liu, W. Clegg, David F.L. Jenkins, and B. Liu, Polarization interferometer for measuring small displacement, IEEE Trans Instrum Meas 50 (2001), 868–871.
2. S.T. Tang and H.-S. Kwok, Characteristics parameters of liquid crystal cells and their measurements, J Display Tech 2 (2006), 26–31.
3. E. Masetti, M. Motecchi, R. Larciprete, and S. Cozzi, In situ monitoring of film deposition with an ellipsometer based on a four-detector photopolarimeter, Appl Opt 35 (1996), 5626–5629.
4. S.G. Nelson, K.S. Johnston, and S.S. Yee, High sensitivity surface plasmon resonance based on phase detection, Sens Actuators B 35/36 (1996), 187–191.
5. T. Keem, S. Gonda, I. Misumi, Q. Huang, and T. Kurosawa, Removing nonlinearity of a homodyne interferometer by adjusting the gains of its quadrature detector system, Appl Opt 43 (2004), 2443–2448.
6. M.W. Wang, F.H. Tsai, and Y.F. Chao, In situ calibration technique for photoelastic modulator in ellipsometry, Thin Solid Films 455/456 (2004), 78–83.
7. F. Pain, R. Coquille, B. Vinouze, N. Wolffer, and P. Gravey, Comparison of twisted and parallel nematic liquid crystal polarization controllers, Application to a 4 × 4 free space optical switch at 1.5 μm, Opt Commun 139 (1997), 199–204.
8. Y. Bitou, Two-wavelength phase-shifting interferometry using an electrically addressed liquid crystal spatial light modulator, Opt Commun 242 (2004), 1–6.

NOVEL REFLECTOR-BACKED FRESNEL ZONE PLATE ANTENNA

S. M. Stout-Grandy,[1] A. Petosa,[2] I. V. Minin,[3] O. V. Minin,[3] and J. S. Wight[1]

[1] Department of Electronics, Carleton University, 1125 Colonel By Drive, Ottawa, Ontario, Canada K1S 5B6; Corresponding author: sstout@doe.carleton.ca

[2] Advanced Antenna Research Group, Communications Research Centre Canada, 3701 Carling Ave., Ottawa, Canada K2H 8S2

[3] Department of Information Protection, Novosibirsk State Technical University (NSTU), 20 Karl Marx Prospect, Novosibirsk 630092, Russia

Received 23 May 2007

ABSTRACT: *A novel reflector-backed Fresnel zone plate antenna (FZPA) is presented. The reflector is positioned at the aperture of the feed antenna such that the radiation that was reflected back off the metal zones of the FZPA gets reradiated instead of being lost. This structure enhances the directivity of the FZPA by about 1 dB and also improves the sidelobes and aperture efficiency. The other benefit of the structure is that it enables a significant reduction in the volume of the FZPA.* © 2007 Wiley Periodicals, Inc. Microwave Opt Technol Lett 49: 3096–3098, 2007; Published online in Wiley InterScience (www.interscience.wiley.com). DOI 10.1002/mop.22946

Key words: *Fresnel zone plate antenna; reflector; millimeter-wave antennas*

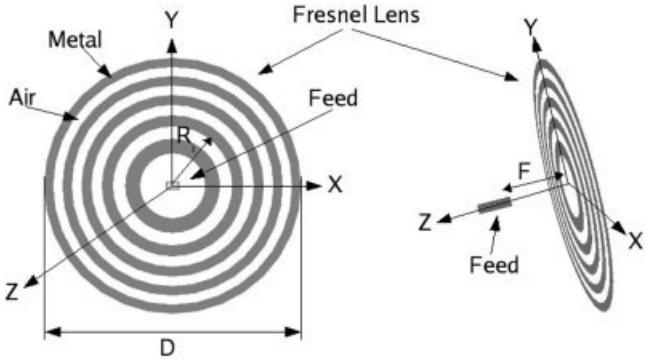

Figure 1 Conventional FZPA in transmission mode

1. INTRODUCTION

A conventional Fresnel zone plate antenna (FZPA) is shown in Figure 1. The planar aperture of the FZPA consists of circular zones which alternate between air and metal. The FZPA is illuminated by a feed antenna located along the z-axis at a distance F from the aperture plane. The metal zones represent the locations on the surface of the aperture where the electromagnetic (EM) waves from the source are 180° out-of-phase relative to the center of the aperture. The metal zones block the out-of-phase waves while the waves that hit the transparent (air) zones diffract through and combine constructively to collimate a beam in the far field [1].

In the Ka-band, FZPAs offer significant practical advantages over shaped lenses, parabolic reflectors, and planar arrays. They are less complex to fabricate, have a reduced aperture profile, are lighter weight, and are less expensive. However, the conventional FZPA has two disadvantages. The first is the inherently low aperture efficiency, which is a result of the significant amount of EM waves that are blocked by the metal zones. The second disadvantage is the large overall volume of the antenna because of the location of the feed relative to the aperture. Several methods have been developed over the last few decades to improve the aperture efficiency of the FZPA [2-6]. One method of particular interest involved a reflecting surface placed a quarter wavelengths behind the FZPA aperture. This effectively converted the antenna into a reflector, similar to a parabolic antenna, and enhanced the aperture efficiency by about twofold [5-7]. This structure is shown in Figure 2(b) compared with the conventional transmission mode version in Figure 2(a). Despite this improvement, however, the reflecting FZPA still suffers from the same large volume as the

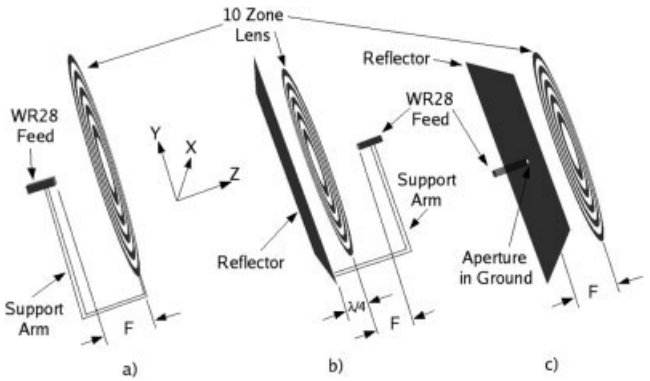

Figure 2 FZPA in (a) Conventional transmission mode, (b) reflection mode, (c)transmission mode with reflector